Check for updates

Elucidation of the role of guanidinium incorporation in single-crystalline MAPbI₃ perovskite on ion migration and activation energy†

Apurba Mahapatra, [ID] [a] Rashmi Runjhun,[b] Jan Nawrocki,[b] Janusz Lewiński, [ID] [bc] Abul Kalam,[d] Pawan Kumar,[a] Suverna Trivedi,[e] Mohammad Mahdi Tavakoli, [ID] [f] Daniel Prochowicz [ID] *[b] and Pankaj Yadav [ID] *[g]

Ion migration plays a significant role in the overall stability and power conversion efficiency of perovskite solar cells (PSCs). This process was found to be influenced by the compositional engineering of the A-site cation in the perovskite crystal structure. However, the effect of partial A-site cation substitution in a methylammonium lead iodide (MAPbI₃) perovskite on the ion migration process and its activation energy is not fully understood. Here we study the effect of a guanidinium (GUA) cation on the ion transport dynamics in the single crystalline GUA$_x$MA$_{1-x}$PbI₃ perovskite composition using temperature-dependent electrochemical impedance spectroscopy (EIS). We find that the small substitution of MA with GUA decreases the activation energy for iodide ion migration in comparison to pristine MAPbI₃. The presence of a large GUA cation in the 3D perovskite structure induces lattice enlargement, which perturbs the atomic interactions within the perovskite lattice. Consequently, the GUA$_x$MA$_{1-x}$PbI₃ crystal exhibits a higher degree of hysteresis during current–voltage (*J*–*V*) measurements than the single-crystalline MAPbI₃ counterpart. Our results provide the fundamental understanding of hysteresis, which is commonly observed in GUA-based PSCs and a general protocol for in-depth electrical characterization of perovskite single crystals.

Introduction

Hybrid organic–inorganic lead halide perovskites have inspired researchers in the field of optoelectronic devices over the last years due to their excellent light absorption, long diffusion length, great photovoltaic (PV) properties, and low-cost processing.[1] These properties extend the scope of application of perovskites in tandem solar cells,[2] photodetectors[3–6] and light-emitting diodes.[7–9] Apart from these encouraging factors, many important challenges in the perovskite semiconductors such as low operational stability,[10] polarization at low frequencies/long time scales,[11,12] and instability to humidity, light exposure and high temperature restrict the commercialization of the PSCs.[13] In addition, ion migration is regarded as the main issue that increases the current–voltage (*J*–*V*) hysteresis[14,15] and reduces the stability of PV devices.[15–17]

The migration process of ions in perovskite films has been intensively studied using photo-thermal induced resonance (PTIR) microscopy,[18] temperature-dependent impedance spectroscopy,[19,20] Muon spin relaxation (μSR),[19] defect spectroscopy,[21] current–potential curves[22,23] and Kelvin probe force microscopy (c-KFM).[24] There are several ions that act as migrating ions in the prototypical MAPbI₃ perovskite *i.e.*, (i) methylammonium (MA), (ii) iodide and (iii) proton or hydrogen ions (H⁺).[15,25,26] The H⁺ ions play a considerably minor role in comparison with other ions due to their low concentration in PSCs.[25,27] Moreover, Pb²⁺ migration within the perovskite structure is hindered due to its high activation energy.[28,29] Thus, MA and iodide ions are primarily migrating ions that affects the stability and hysteresis of PV devices

[a] *Department of Physics & Astronomy, National Institute of Technology, Rourkela, 769008, India*

[b] *Institute of Physical Chemistry, Polish Academy of Sciences, Kasprzaka 44/52, 01-224 Warsaw, Poland. E-mail: dprochowicz@ichf.edu.pl*

[c] *Faculty of Chemistry, Warsaw University of Technology, Noakowskiego 3, 00-664 Warsaw, Poland*

[d] *Department of Chemistry, Faculty of Science, King Khalid University, P.O. Box 9004, Abha 61413, Saudi Arabia*

[e] *Department of Chemical Engineering, National Institute of Technology, Rourkela, 769008, India*

[f] *Department of Electrical Engineering and Computer Science, Massachusetts Institute of Technology, Cambridge, MA 02139, USA*

[g] *Department of Solar Energy, School of Technology, Pandit Deendayal Petroleum University, Gandhinagar-382 007, Gujarat, India. E-mail: Pankajphd11@gmail.com*

† Electronic supplementary information (ESI) available. See DOI: 10.1039/d0cp01119c

This journal is © the Owner Societies 2020

Phys. Chem. Chem. Phys., 2020, **22**, 11467–11473 | 11467

due to their low activation energy to move through the perovskite structure (0.5–0.8 eV for MA and 0.2–0.7 eV for iodide ions).[20,23,28,30–33] Moreover, the observed hysteresis in perovskite solar cells (PSCs) is ascribed to the iodide ion because it has a diffusion coefficient of 10^{-12} cm^2 s^{-1}, which is 5 times larger than that of MA cations (10^{-16} cm^2 s^{-1}).[14,32] By controlling the chemical composition and surface passivation of the perovskite film, the ion motion through the perovskite lattice can be retarded, leading to improved stability and suppressed J–V hysteresis.[31,34] For example, the performance, and stability of PSCs are improved, when a part of iodide ions is replaced by smaller bromide ions, which show stronger hydrogen-bonding interactions with the organic ammonium cations[35,36] due to higher electronegativity (Mulliken, bromide: 6.76, iodide: 4.24) or hardness (bromide: 4.24, iodide: 3.70).[35,37] On the other hand, the stability, and efficiency of PSCs can be enhanced by substitution of MA cations with formamidinium (FA), azetidinium (Az) or guanidinium (GUA) cations.[19,38–40] As theoretically studied, GUA cations show potential to solve the hysteresis issue in the PSCs due to its zero dipole moment and larger size of 278 pm as compared to the MA cation (217 pm).[41,42] Surprisingly, it was found that the incorporation of GUA in the MAPbI$_3$ perovskite structure enhances the hysteresis effect in comparison to the pristine MAPbI$_3$ based PSCs.[38,43] Initially, Yang *et al.* assumed that GUA is not confined within the perovskite lattice but rather is weakly hydrogen-bonded to the under-coordinated ionic species mainly at grain boundaries.[38] They proposed that mobile GUA cations can migrate to the interfaces and screen the applied electric field leading to enhanced hysteresis in the device. However, more recent studies revealed that GUA is able to replace MA cations forming a pure phase of the GUA$_x$MA$_{1-x}$PbI$_3$-type perovskite.[40,44] Under these circumstances, the determination of the precise effect of GUA incorporation into the MAPbI$_3$ perovskite lattice on the ionic migration needs further investigations. Notably, the mentioned studies concerned the investigation of completed devices, where the ion motions can be influenced by the grain boundaries in the perovskite active layer, interfaces of the absorber layer with the electron and hole transporting layers and aging of the solar cells. The presence of grain boundaries provides fast paths for the migration of ions leading to a higher hysteresis and lower stability. Thus, the elucidation of the exact role of the cations and halides on the ion migration process by investigating the polycrystalline perovskite films has not been achieved.

In this work, we study the effect of GUA on ion transport in mixed-cation GUA$_x$MA$_{1-x}$PbI$_3$ perovskite single crystals using temperature-dependent electrochemical impedance spectroscopy (EIS). The investigation of single crystals allows elimination of the effect of grain boundaries and interfaces on the kinetics of ion migration, and it is crucial to study the intrinsic behavior of perovskite semiconductors for a better understanding of the charge transport and recombination phenomena. We show that the GUA$_x$MA$_{1-x}$PbI$_3$ perovskite single crystals exhibit lower activation energy for the iodide ion migration than MAPbI$_3$ single crystals. The GUA$_x$MA$_{1-x}$PbI$_3$ single crystals also exhibit a higher degree of hysteresis during current–voltage (J–V)

measurements than the single-crystalline MAPbI$_3$ counterparts, demonstrating higher ionic motion in the GUA$_x$MA$_{1-x}$PbI$_3$ perovskite system. These results provide a basic insight into the precise effect of the GUA incorporation into the MAPbI$_3$ perovskite lattice on the ion migration process.

Results and discussion

MAPbI$_3$ and GUA$_x$MA$_{1-x}$PbI$_3$ perovskite single crystals were synthesized using the inverse temperature crystallization method in γ-butyrolactone.[45] In the case of GUA$_x$MA$_{1-x}$PbI$_3$ single crystals, a 1 M precursor solution containing PbI$_2$, MAI and GUAI with the molar ratio of 1:0.8:0.2 were employed (for details see the Experimental section). The ratio of the organic cations incorporated into the perovskite structure was estimated using liquid-state ^{1}H NMR analysis by dissolving one separate crystal in 500 μL of DMSO-d$_6$. By comparing the integrals of the MA and GUA peaks, we find that the actual MA/GUA ratio is 0.985:0.015, which remarkably differs from the nominal ratio in the solution (Fig. S1, ESI†). Three crystals from the same batch were measured and the results show the same ratio with a low concentration of GUA in the perovskite crystals. The high discrepancy in the GUA content between the actual and nominal GUA/MA ratio in crystal and solution is likely due to the very low yield of the crystallization process (~10%), which can be attributed to the high solubility of the perovskite precursors. We also attempted the synthesis of GUA$_x$MA$_{1-x}$PbI$_3$ single crystals containing a higher GUA content by mixing PbI$_2$, MAI and GUAI with the molar ratios of 1:0.7:0.3 and 1:0.6:0.4, but using the above-mentioned procedure, we failed to crystallize the materials as single crystals. Thus, the crystals with the formula GUA$_{0.015}$MA$_{0.985}$PbI$_3$ (GUAMA) were used to further study the properties of GUA-based perovskite crystals. Powder X-ray diffraction (pXRD) measurements were performed on the resulting MAPbI$_3$ and GUAMA crystals to check the structure and phase purity. As shown in Fig. S2 (ESI†), both samples display a similar perovskite crystal structure with diffraction peaks centered at 14.07°, 28.1°, and 31.8°.[46] We observed a small shift of the diffraction peaks to lower angles upon introduction of GUA cations, which is in accordance with the literature.[40,44] Next, thin layers of silver (Ag) were deposited on both sides of MAPbI$_3$ and GUAMA crystals with dimensions of 4 × 4 × 1.92 mm and 1.7 × 1.7 × 1.2 mm (Fig. S3, ESI†), respectively.

In order to calculate the activation energy of ions, we performed electrochemical impedance spectroscopy (EIS) measurements as a function of temperature in the frequency range from 1 MHz to 1 Hz at an AC perturbation voltage of 20 mV under dark conditions. Fig. 1a and b show the EIS Nyquist spectra of both MAPbI$_3$ and GUAMA single crystals at different temperatures. To check the thermal stability of the investigated crystals, the EIS measurements as a function of decreasing temperature were also measured (Fig. S4, ESI†). We found that the EIS spectra recorded during both measurement cycles exhibit a similar behavior, which signifies that the perovskite
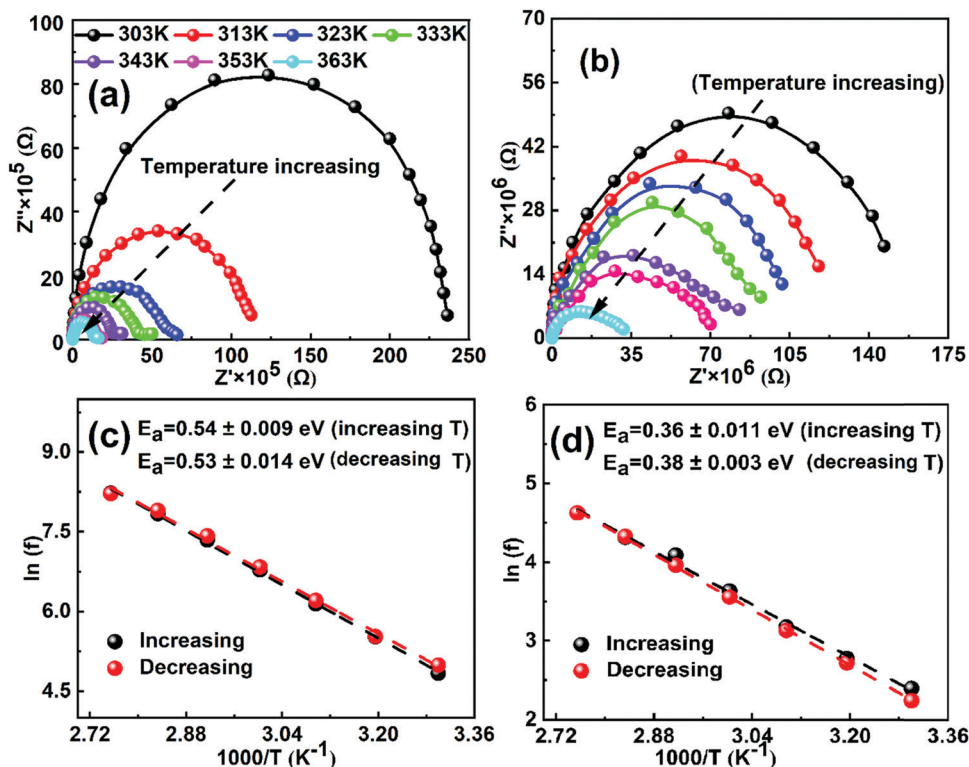
11468 | *Phys. Chem. Chem. Phys.*, 2020, **22**, 11467–11473

This journal is © the Owner Societies 2020

Fig. 1 Nyquist plots of the (a) MAPbI$_3$ and (b) GUA$_{0.015}$MA$_{0.985}$PbI$_3$ single crystals at 0 V DC bias in the frequencies ranging from 1 MHz to 1 Hz as a function of temperature (313–363 K). Arrhenius plots of the inflection frequencies vs. 1000/T (ln(f_0) vs. 1000/T) during increasing and decreasing temperature of (c) MAPbI$_3$ and (d) GUA$_{0.015}$MA$_{0.985}$PbI$_3$ crystals. E_a is the activation energy for the traps.

crystals are thermally stable in the temperature range of 303–363 K. Notably, the obtained Nyquist spectra of both crystals show a single semicircle, which is consistent with our recent report.[47] However, two or three semicircles corresponding to the high, mid and low-frequency regions are observed for PSCs. The interpretation of these semicircles is usually explained with the help of an electrical equivalent circuit, which is still controversial in the literature. Nevertheless, it is generally acceptable to ascribe the mid or low frequency (from 1 to 10^3 Hz) response to ion motion. In the present work, Nyquist spectra of both crystals decrease with increasing temperature due to the increase in the conductivity. The rate of change in the real part of Nyquist spectra is found to be higher for MAPbI$_3$ than that of GUA$_x$MA$_{1-x}$PbI$_3$ crystals (Fig. S5, ESI†). The higher rate of change in real part of Nyquist spectra for MAPbI$_3$ crystal signifies its lower temperature stability.

Fig. S6 (ESI†) shows the plots of the complex part of impedance as functions of frequency and temperature. The peaks in the complex impedance spectra at frequencies ranging from 10^1 to 10^3 Hz and 10^1 to 10^2 Hz are clearly visible for MAPbI$_3$ and GUA$_x$MA$_{1-x}$PbI$_3$ crystals, respectively. The observed frequency ranges and corresponding time constant is on the same order as the low frequency response in PSCs, which suggests that the net response of perovskite crystals is due to the ion migration. In our previous reports on GUA$_x$MA$_{1-x}$PbI$_3$ PSCs, we observed a complex impedance peak between 10^5 and 10^6 Hz and the

corresponding time constant depicts the recombination kinetics in the cell, which is significantly suppressed upon GUA incorporation.[43,48] However, such high-frequency response is not observed in the present study. In turn, we observed that with incorporation of a small amount of the GUA cation in the MAPbI$_3$ crystal structure, the rate of change in the apparent time constant is significantly suppressed with a change in temperature. The higher apparent time constant is found to be associated with the hysteresis phenomenon in PSCs.[49] The activation energies were extracted from the apparent time constant for both crystals as a function of increasing and decreasing temperature and plotted in Fig. 1c and d. The activation energy of 0.53 and 0.36 eV is found for MAPbI$_3$ and GUAMA, respectively, which is consistent with our[47] and other group's results.[38] The lower activation energy of the GUAMA crystal signifies that ion migration occurred more easily in this crystal in comparison with the pristine MAPbI$_3$. The activation energy of ions calculated for both MAPbI$_3$ and GUA$_x$MA$_{1-x}$PbI$_3$ thin films using EIS and temperature-dependent ion conductivity are summarized in Table 1.

Most of the values for MAPbI$_3$ and GUA$_x$MA$_{1-x}$PbI$_3$ thin films are found in the range of 0.3–0.6 eV and 0.1 to 0.7 eV, respectively. For example, Yang et al., have calculated an activation energy of 21.11 meV for MAPbI$_3$ PSC and a significantly lower activation energy of 14.86 meV for GUA$_x$MA$_{1-x}$PbI$_3$ devices.[38] This indicates that the recombination within the bulk of the perovskite film has been successfully suppressed.

This journal is © the Owner Societies 2020

Phys. Chem. Chem. Phys., 2020, **22**, 11467–11473 | **11469**

Table 1 Calculated values of activation energy of ions for MAPbI$_3$ and GUA$_x$MA$_{1-x}$PbI$_3$ by EIS and temperature-dependent ion conductivity measurements

Activation energy of ions for MAPbI$_3$ and GUA$_x$MA$_{1-x}$PbI$_3$

|	Activation Energy	Measurements	Ref.
MAPbI$_3$	0.624 eV (I$^-$) (single crystal)	Temperature-dependent ion conductivity	50
	0.82 eV (thin film)	Temperature-dependent ion conductivity	51
	0.53 eV (I$^-$)	Temperature-dependent electrochemical impedance spectroscopy (EIS)	30
	0.51 eV (I$^-$)	Temperature-dependent ion conductivity from Warburg impedance	30
	1.05 eV (single crystal)	Temperature-dependent ion conductivity	31
	0.5 eV (thin film)		
	0.43 eV (I$^-$) (pellets)	Temperature-dependent ion conductivity	52
MAPbI$_3$	0.0211 eV (thin film)	AdmittanceSpectroscopy	38
MA$_{0.95}$GA$_{0.05}$PbI$_3$	0.0148 eV		
MAPbI$_3$	0.29 eV (thin film)	Temperature-dependent electrochemical impedance spectroscopy (EIS)	19
MA$_{0.95}$GA$_{0.05}$PbI$_3$	0.38 eV		
	Mid frequency (1 Hz–10^5 Hz)		
MAPbI$_3$	0.4 eV		
MA$_{0.95}$GA$_{0.05}$PbI$_3$	N/A		
	Low frequency ($>$1 Hz)		

In turn, Ferdani et al., calculated an activation energy of 0.44 eV for the MAPbI$_3$ PSC by plotting the EIS low-frequency time constant as a function of temperature.[19] The obtained activation energy is close to our calculation and is mainly found to be associated with the diffusion of iodide ions. The activation energy for the GUA$_{0.05}$MA$_{0.95}$PbI$_3$ PSC has not been derived from EIS, however, the value of 0.78 eV was obtained from Ab initio simulation, which is comparatively higher with respect to our values and the reported values by Yang et al.[38]

To further confirm the values of activation energies derived from EIS measurements, the conductivity of perovskite crystals was measured under dark conditions (Fig. S7, ESI†) and plotted in the Nerst–Einstien formalism (Fig. 2). It is well-established for mixed conductors that ionic conduction is dominant in the high-temperature region, while electronic conduction is dominant in the low-temperature region.[53] From the obtained plot, the activation energy is derived using the expression of $\sigma \cdot T = \sigma_0 \exp\left(-\frac{E_a}{k_B T}\right)$, where k_B is the Boltzman constant, T is the absolute temperature and σ_0 is a constant.[54] By using the Arrhenius plot, the activation energies of 0.52 and 0.36 eV are obtained for MAPbI$_3$ and GUAMA crystals, respectively. The obtained activation energies are in good agreement with our

EIS findings. For metal halide perovskites, iodide vacancies have been found to have a more detrimental influence on the charge trapping and non-radiative recombination because of their deep energy levels.

The ion activation energy is also defined as a result of the interaction between the ion and the perovskite lattice. This interaction can be easily tuned by the substitution of the halide or A-site cations in the perovskite structure. In our previous works, using solid-state NMR, we showed that when MA with a radius of 2.17 Å is substituted by a cation with larger ionic radius, i.e., FA (2.53 Å)[55] or GUA (2.78 Å),[40] these organic groups exhibit a higher degree of rotation. This behavior can cause an additional strain and weaken the atomic interaction inside the lattice and consequently decrease the ion activation energy (see Fig. 3).[56] However, the substitution of the A-site cation with a lower radius cation, e.g. Rb (1.52 Å) or Cs (1.67 Å), compresses the perovskite lattice and suppresses the ion motion.[57] For instance, Zhou et al., have shown that Cs-based perovskites possess higher ion activation energy as compared to MA-based ones, which led to better light stability.[58]

The suppression of ion migration with increasing ion activation energy can be easily observed during current–voltage (I–V) measurement at different scan rates. Fig. S8 (ESI†) shows the
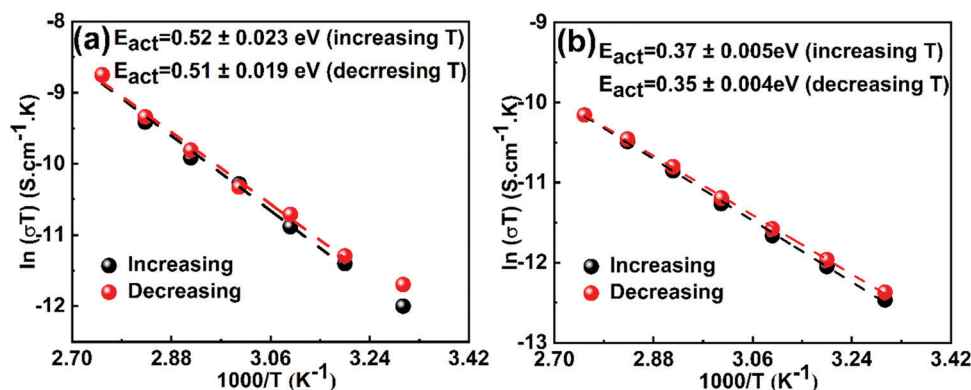
Fig. 2 Temperature-dependent conductivity of (a) MAPbI$_3$ and (b) GUA$_{0.015}$MA$_{0.985}$PbI$_3$ single crystals (Arrhenius plot).

11470 | Phys. Chem. Chem. Phys., 2020, **22**, 11467–11473
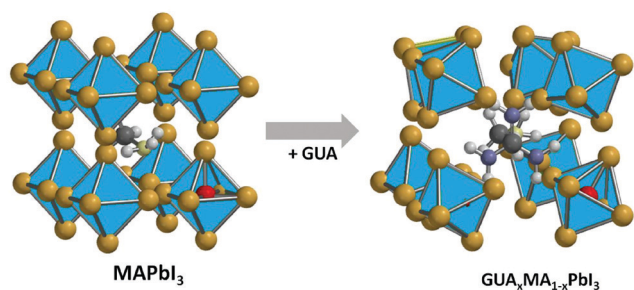
This journal is © the Owner Societies 2020

Fig. 3 Schematic representation of the introduction of the GUA cation into the MAPbI$_3$ crystal lattice.

hysteresis behavior of both crystals at different scan rates. A higher hysteresis effect is observed for the GUAMA crystal, which confirms the higher ionic motion in the GUA$_x$MA$_{1-x}$PbI$_3$ perovskite systems.[19,42,44]

Conclusions

The effect of GUA incorporation into the MAPbI$_3$ perovskite lattice on the ion transport properties has been investigated using a combination of electrochemical impedance spectroscopy (EIS) and temperature-dependent ion conductivity techniques. This study provides the first insights into the effect on iodide ion transport in the GUA$_x$MA$_{1-x}$PbI$_3$ single crystal. The calculated average activation energy corresponding to the ion migration for MAPbI$_3$ and GUA$_x$MA$_{1-x}$PbI$_3$ crystals are 0.52 and 0.36 eV, respectively. The substitution of MA with GUA cations in the MAPbI$_3$ crystal lattice is found to cause an additional strain and weaken the atomic interaction inside the lattice. This consequently decreases the ion activation energy of MAPbI$_3$ crystals. The present study enhances our fundamental understanding of ion migration and provides a basic insight into the mixed-cation perovskite single crystals.

Experimental section

Synthesis of MAPbI$_3$ and GUA$_x$MA$_{1-x}$PbI$_3$ single crystals

1.0 M MAPbI$_3$ solution was prepared by dissolving equimolar amounts of PbI$_2$ and MAI in γ-butyrolactone at 60 °C overnight. Similarly, perovskite solution containing PbI$_2$, MAI and GUAI in a molar ratio of 1 : 0.8 : 0.2 was prepared in γ-butyrolactone and kept at 60 °C overnight. Before crystallization, the solution was filtered using 0.2 μm pore size PTFE filter. Next, 2 mL filtered precursor solution was kept at 160 °C for 30 min in an oil bath, which resulted in the growth of very small seed crystals. The seed crystal solution was further heated at 120 °C for 3 h. Finally, the remaining solution was discarded, and crystals were washed with acetone 2–3 times and then dried.

Characterization of perovskite single crystals

The ^{1}H NMR spectra were recorded at 298 K on a Bruker 600 AVANAC III spectrometer and the spectra were analyzed using Nova software. Powder X-ray diffraction patterns were recorded with a Empyrean diffractometer (PANalytical) equipped with a copper lamp (40 kV, 40 mA). The pXRD patterns were recorded for finely ground crystals over a 2θ range of 10° to 40° without rotating the sample using a low background Si sample holder. EIS and temperature-dependent ion conductivity measurements were performed using a potentiostat (Autolab) equipped with a frequency response analyzer. EIS measurements were performed as a function of temperature.

Conflicts of interest

There are no conflicts to declare.

Acknowledgements

References

1 A. Mahapatra, D. Prochowicz, M. M. Tavakoli, S. Trivedi, P. Kumar and P. Yadav, *J. Mater. Chem. A*, 2019, **8**, 27–54.

2 G. E. Eperon, T. Leijtens, K. A. Bush, R. Prasanna, T. Green, J. T.-W. W. Wang, D. P. McMeekin, G. Volonakis, R. L. Milot, R. May, A. Palmstrom, D. J. Slotcavage, R. A. Belisle, J. B. Patel, E. S. Parrott, R. J. Sutton, W. Ma, F. Moghadam, B. Conings, A. Babayigit, H.-G. G. Boyen, S. Bent, F. Giustino, L. M. Herz, M. B. Johnston, M. D. McGehee and H. J. Snaith, *Science*, 2016, **354**, 861–865.

3 Y. Guo, C. Liu, H. Tanaka and E. Nakamura, *J. Phys. Chem. Lett.*, 2015, **6**, 535–539.

4 H. Deng, X. Yang, D. Dong, B. Li, D. Yang, S. Yuan, K. Qiao, Y.-B. Cheng, J. Tang and H. Song, *Nano Lett.*, 2015, **15**, 7963–7969.

5 L. Dou, Y. Yang, J. You, Z. Hong, W.-H. Chang, G. Li and Y. Yang, *Nat. Commun.*, 2014, **5**, 5404.

6 K. Pandey, M. Chauhan, V. Bhatt, B. Tripathi, P. Yadav and M. Kumar, *RSC Adv.*, 2016, **6**, 105076–105080.

7 O. A. Jaramillo-Quintero, R. S. Sanchez, M. Rincon and I. Mora-Sero, *J. Phys. Chem. Lett.*, 2015, **6**, 1883–1890.

8 N. K. Kumawat, D. Gupta and D. Kabra, *Energy Technol.*, 2017, **5**, 1734–1749.

9 Z.-K. Tan, R. S. Moghaddam, M. L. Lai, P. Docampo, R. Higler, F. Deschler, M. Price, A. Sadhanala, L. M. Pazos, D. Credgington, F. Hanusch, T. Bein, H. J. Snaith and R. H. Friend, *Nat. Nanotechnol.*, 2014, **9**, 687–692.

10 T. A. Berhe, W.-N. Su, C.-H. Chen, C.-J. Pan, J.-H. Cheng, H.-M. Chen, M.-C. Tsai, L.-Y. Chen, A. A. Dubale and B.-J. Hwang, *Energy Environ. Sci.*, 2016, **9**, 323–356.

11 E. J. Juarez-Perez, R. S. Sanchez, L. Badia, G. Garcia-Belmonte, Y. S. Kang, I. Mora-Sero and J. Bisquert, *J. Phys. Chem. Lett.*, 2014, **5**, 2390–2394.

12 Z. Xiao, Y. Yuan, Y. Shao, Q. Wang, Q. Dong, C. Bi, P. Sharma, A. Gruverman and J. Huang, *Nat. Mater.*, 2015, **14**, 193–198.

13 P. Zhao, B. J. Kim and H. S. Jung, *Mater. Today Energy*, 2018, **7**, 267–286.

14 M. De Bastiani, G. Dell'Erba, M. Gandini, V. D'Innocenzo, S. Neutzner, A. R. S. Kandada, G. Grancini, M. Binda, M. Prato, J. M. Ball, M. Caironi and A. Petrozza, *Adv. Energy Mater.*, 2016, **6**, 1501453.

15 M. L. Petrus, J. Schlipf, C. Li, T. P. Gujar, N. Giesbrecht, P. Müller-Buschbaum, M. Thelakkat, T. Bein, S. Hüttner and P. Docampo, *Adv. Energy Mater.*, 2017, **7**, 1700264.

16 J. Carrillo, A. Guerrero, S. Rahimnejad, O. Almora, I. Zarazua, E. Mas-Marza, J. Bisquert and G. Garcia-Belmonte, *Adv. Energy Mater.*, 2016, **6**, 1502246.

17 M. Bag, L. A. Renna, R. Y. Adhikari, S. Karak, F. Liu, P. M. Lahti, T. P. Russell, M. T. Tuominen and D. Venkataraman, *J. Am. Chem. Soc.*, 2015, **137**, 13130–13137.

18 Y. Yuan, J. Chae, Y. Shao, Q. Wang, Z. Xiao, A. Centrone and J. Huang, *Adv. Energy Mater.*, 2015, **5**, 1500615.

19 D. W. Ferdani, S. R. Pering, D. Ghosh, P. Kubiak, A. B. Walker, S. E. Lewis, A. L. Johnson, P. J. Baker, M. S. Islam and P. J. Cameron, *Energy Environ. Sci.*, 2019, **12**, 2264–2272.

20 A. Pockett, G. E. Eperon, N. Sakai, H. J. Snaith, L. M. Peter and P. J. Cameron, *Phys. Chem. Chem. Phys.*, 2017, **19**, 5959–5970.

21 Y. Hu, E. M. Hutter, P. Rieder, I. Grill, J. Hanisch, M. F. Aygüler, A. G. Hufnagel, M. Handloser, T. Bein, A. Hartschuh, K. Tvingstedt, V. Dyakonov, A. Baumann, T. J. Savenije, M. L. Petrus and P. Docampo, *Adv. Energy Mater.*, 2018, **8**, 1703057.

22 S. Meloni, T. Moehl, W. Tress, M. Franckeviius, M. Saliba, Y. H. Lee, P. Gao, M. K. Nazeeruddin, S. M. Zakeeruddin, U. Rothlisberger and M. Graetzel, *Nat. Commun.*, 2016, **7**, 10334.

23 I. Levine, P. K. Nayak, J. T.-W. Wang, N. Sakai, S. Van Reenen, T. M. Brenner, S. Mukhopadhyay, H. J. Snaith, G. Hodes and D. Cahen, *J. Phys. Chem. C*, 2016, **120**, 16399–16411.

24 J. S. Yun, J. Seidel, J. Kim, A. M. Soufiani, S. Huang, J. Lau, N. J. Jeon, S. Il Seok, M. A. Green and A. Ho-Baillie, *Adv. Energy Mater.*, 2016, **6**, 1600330.

25 J. M. Frost and A. Walsh, *Acc. Chem. Res.*, 2016, **49**, 528–535.

26 Y. Yuan and J. Huang, *Acc. Chem. Res.*, 2016, **49**, 286–293.

27 D. A. Egger, L. Kronik and A. M. Rappe, *Angew. Chem., Int. Ed.*, 2015, **54**, 12437–12441.

28 J. M. Azpiroz, E. Mosconi, J. Bisquert and F. De Angelis, *Energy Environ. Sci.*, 2015, **8**, 2118–2127.

29 N. K. Elumalai, M. A. Mahmud, D. Wang and A. Uddin, *Energies*, 2016, **9**, 861.

30 M. N. F. Hoque, N. Islam, Z. Li, G. Ren, K. Zhu and Z. Fan, *ChemSusChem*, 2016, **9**, 2692–2698.

31 J.-W. W. Lee, S.-G. G. Kim, J.-M. M. Yang, Y. Yang and N.-G. G. Park, *APL Mater.*, 2019, **7**, 041111.

32 C. Eames, J. M. Frost, P. R. F. Barnes, B. C. O'Regan, A. Walsh and M. S. Islam, *Nat. Commun.*, 2015, **6**, 7497.

33 Y. Yuan, Q. Wang, Y. Shao, H. Lu, T. Li, A. Gruverman and J. Huang, *Adv. Energy Mater.*, 2016, **6**, 1501803.

34 A. Mahapatra, D. Prochowicz, M. M. Tavakoli, S. Trivedi, P. Kumar and P. Yadav, *J. Mater. Chem. A*, 2020, **8**, 27–54.

35 R. Ruess, F. Benfer, F. Böcher, M. Stumpp and D. Schlettwein, *ChemPhysChem*, 2016, **17**, 1505–1511.

36 J. H. Noh, S. H. Im, J. H. Heo, T. N. Mandal and S. I. Seok, *Nano Lett.*, 2013, **13**, 1764–1769.

37 R. G. Parr and R. G. Pearson, *J. Am. Chem. Soc.*, 1983, **105**, 7512–7516.

38 N. De Marco, H. Zhou, Q. Chen, P. Sun, Z. Liu, L. Meng, E. P. Yao, Y. Liu, A. Schiffer and Y. Yang, *Nano Lett.*, 2016, **16**, 1009–1016.

39 S. R. Pering, W. Deng, J. R. Troughton, P. S. Kubiak, D. Ghosh, R. G. Niemann, F. Brivio, F. E. Jeffrey, A. B. Walker, M. S. Islam, T. M. Watson, P. R. Raithby, A. L. Johnson, S. E. Lewis and P. J. Cameron, *J. Mater. Chem. A*, 2017, **5**, 20658–20665.

40 D. J. Kubicki, D. Prochowicz, A. Hofstetter, M. Saski, P. Yadav, D. Bi, N. Pellet, J. Lewiński, S. M. Zakeeruddin, M. Grätzel and L. Emsley, *J. Am. Chem. Soc.*, 2018, **140**, 3345–3351.

41 G. Giorgi, J.-I. I. Fujisawa, H. Segawa and K. Yamashita, *J. Phys. Chem. C*, 2015, **119**, 4694–4701.

42 G. Giorgi and K. Yamashita, *Nanotechnology*, 2015, **26**, 442001.

43 D. Prochowicz, M. M. Tavakoli, A. Q. Alanazi, S. Trivedi, H. Tavakoli Dastjerdi, S. M. Zakeeruddin, M. Grätzel and P. Yadav, *ACS Omega*, 2019, **4**, 16840–16846.

44 A. D. Jodlowski, C. Roldán-Carmona, G. Grancini, M. Salado, M. Ralaiarisoa, S. Ahmad, N. Koch, L. Camacho, G. D. Miguel and M. K. Nazeeruddin, *Nat. Energy*, 2017, **2**, 972–979.

45 J. Burschka, N. Pellet, S.-J. Moon, R. Humphry-Baker, P. Gao, M. K. Nazeeruddin and M. Grätzel, *Nature*, 2013, **499**, 316–319.

46 Z. Lian, Q. Yan, Q. Lv, Y. Wang, L. Liu, L. Zhang, S. Pan, Q. Li, L. Wang and J. L. Sun, *Sci. Rep.*, 2015, **5**, 16563.

47 A. Kalam, R. Rashmi, M. Apurba, M. M. Tavakoli, T. Suverna, H. T. Dastjerdi, K. Pawan, J. Lewiński, M. Pandey, D. Prochowicz and P. Yadav, *J. Phys. Chem. C*, 2020, **124**, 3496–3502.

48 D. Prochowicz, M. M. Tavakoli, A. Kalam, R. D. Chavan, S. Trivedi, M. Kumar and P. Yadav, *J. Mater. Chem. A*, 2019, **7**, 8218–8225.

49 F. Ebadi, N. Taghavinia, R. Mohammadpour, A. Hagfeldt and W. Tress, *Nat. Commun.*, 2019, **10**, 1574.

11472 | *Phys. Chem. Chem. Phys.*, 2020, **22**, 11467–11473

This journal is © the Owner Societies 2020

50 S. Yang, S. Chen, E. Mosconi, Y. Fang, X. Xiao, C. Wang, Y. Zhou, Z. Yu, J. Zhao, Y. Gao, F. De Angelis and J. Huang, *Science*, 2019, **365**, 473–478.

51 Y. C. Zhao, W. K. Zhou, X. Zhou, K. H. Liu, D. P. Yu and Q. Zhao, *Light: Sci. Appl.*, 2017, **6**, e16243.

52 T.-Y. Yang, G. Gregori, N. Pellet, M. Grätzel and J. Maier, *Angew. Chem., Int. Ed.*, 2015, **54**, 7905–7910.

53 H. Lee, S. Gaiaschi, P. Chapon, D. Tondelier, J. E. Bourée, Y. Bonnassieux, V. Derycke and B. Geffroy, *J. Phys. Chem. C*, 2019, **123**, 17728–17734.

54 R. A. McKee, *Solid State Ionics*, 1981, **5**, 133–136.

55 D. J. Kubicki, D. Prochowicz, A. Hofstetter, P. Péchy, S. M. Zakeeruddin, M. Grätzel and L. Emsley, *J. Am. Chem. Soc.*, 2017, **139**, 10055–10061.

56 J. Shi, Y. Li, Y. Li, D. Li, Y. Luo, H. Wu and Q. Meng, *Joule*, 2018, **2**, 879–901.

57 M. Saliba, T. Matsui, K. Domanski, J. Y. Seo, A. Ummadisingu, S. M. Zakeeruddin, J. P. Correa-Baena, W. R. Tress, A. Abate, A. Hagfeldt and M. Grätzel, *Science*, 2016, **354**, 206–209.

58 W. Zhou, Y. Zhao, X. Zhou, R. Fu, Q. Li, Y. Zhao, K. Liu, D. Yu and Q. Zhao, *J. Phys. Chem. Lett.*, 2017, **8**, 4122–4128.

This journal is © the Owner Societies 2020

Phys. Chem. Chem. Phys., 2020, **22**, 11467–11473 | 11473